Orbital and Pauli limiting effects in heavily doped Ba_{0.05}K_{0.95}Fe_{2}As_{2}

Shuai Zhang, Y. P. Singh, X. Y. Huang, X. J. Chen, M. Dzero, and C. C. Almasan

Phys. Rev. B **92**, 174524 — Published 20 November 2015

DOI: 10.1103/PhysRevB.92.174524

Orbital and Pauli limiting effects in heavily doped $Ba_{0.05}K_{0.95}Fe_2As_2$

Shuai Zhang,[1] Y. P. Singh,[1] X. Y. Huang,[1] X. J. Chen,[2] M. Dzero,[1,3] and C. C. Almasan[1]

[1] *Department of Physics, Kent State University, Kent, Ohio 44242, USA*
[2] *Center for High Pressure Science and Technology Advanced Research, Shanghai 201203, China*
[3] *Max Planck Institute for Physics of Complex Systems, 01187 Dresden, Germany*

(Dated: October 12, 2015)

We investigated the thermodynamic properties of the Fe-based lightly-disordered superconductor $Ba_{0.05}K_{0.95}Fe_2As_2$ in external magnetic field H applied along the FeAs layers ($H||ab$ planes). The superconducting (SC) transition temperature for this doping level is $T_c = 6.6$ K. Our analysis of the specific heat $C(T,H)$ measured for $T < T_c$ implies a sign change of the superconducting order parameter across different Fermi pockets. We provide experimental evidence for the three components superconducting order parameter. We find that all three components have values which are comparable with the previously reported ones for the stoichiometric compound KFe_2As_2. Our data for $C(T,H)$ and resistivity $\rho(T,H)$ can be interpreted in favor of the dominant orbital contribution to the pair-breaking mechanism at low fields, while Pauli limiting effect dominates at high fields, giving rise to a gapless superconducting state with only the leading non-zero gap.

PACS numbers: 74.25.-q,74.62.bf,74.25.fc

I. INTRODUCTION

Materials with multiple Fermi surfaces may host unconventional superconductivity even for the case when one considers electron-phonon and Coulomb interactions only[1]. Since the interactions between the electrons from the same band as well as between the bands are fixed by the symmetry of the underlying orbitals, the resulting symmetry of a superconducting order parameter does not necessarily have to be of the conventional s-wave type. While more exotic pairing mechanisms such as spin fluctuation exchange mechanism may naturally lead to the realization of exotic superconductivity in multiband materials with d- or f-electronic orbitals, it is generally expected that the microscopic structure of the superconducting order parameter remains universal under pressure or doping.

The discovery of the '122' family of iron-based superconductors[2] has provided an example of unconventional superconductivity with a non-universal gap structure[3–8]. In particular, in the hole-doped $Ba_{1-x}K_xFe_2As_2$ high-T_c superconductor, the superconducting order parameter changes its symmetry with increasing doping level from lightly doped to over-doped regimes: at optimal hole doping ($x = 0.4$), the SC gap symmetry is of $s^{\pm}$ type[9,10] with sign change between the isotropic fully-gapped hole Fermi pockets at the Γ point and electron Fermi pocket at the M point in one Fe Brillouin zone (BZ), while the nodes in the gap appear in heavily-doped alloys as $x \to 1$[11–14]. This property appears to be universal as it is observed in other iron-based superconductor compounds[15–17] and is most likely driven by near degeneracy between the superconducting states with different gap structure[5,6,18–21].

Of a particular interest are the heavily overdoped $Ba_{1-x}K_xFe_2As_2$ compounds. An important feature of these materials is that the electron pockets near the M points are almost completely gone via the topological Lifshitz transition at $x \approx 0.9$, while another hole band appears off-center relative to the BZ corner[11,15,22,23]. Thus, the electronic properties for doping levels just above 90% are mainly governed by the three hole pockets near the Γ point. Importantly, the superconducting critical temperature does not vary significantly for doping levels just below or above the Lifshitz transition[24]. Furthermore, laser-excited angle-resolved photoemission spectroscopy measurements[12] have revealed a highly unusual gap structure in KFe_2As_2 with octet-line nodes on the middle hole Fermi sheet and nodeless gaps on inner and outer Fermi surfaces. In addition, while ARPES[12,24,25], residual thermal conductivity[14], and specific heat[26–28] results support an accidental nodes scenario, thermal conductivity[29,30] and measurements of the changes in the superconducting critical temperature with pressure P in KFe_2As_2[13], which reveal an evolution from a d-wave gap for $P < P_c$ to a $s^{\pm}$ gap for $P > P_c$, strongly support a symmetry protected nodes scenario; impurity scattering effect studied using thermal conductivity[29], London penetration depth[31], and specific heat[32] measurements also supports the scenario of symmetry-protected line nodes. Thus, the gap symmetry with nodes in this system is still an open question.

In this paper we focus on the bulk properties of specific heat in single crystals of $Ba_{0.05}K_{0.95}Fe_2As_2$. In particular, based on the measurements of specific heat performed in the $H||ab$ plane geometry (fixed direction of the magnetic field) we provide experimental evidence for the existence of a three-component superconducting order parameter. Importantly, we find that at least two components have opposite sign. We also discuss the competition between spin and orbital pair breaking effects due to the generation of the Josephson vortices formed with a core running parallel to the FeAs planes. Specifically, our analysis of the field dependence of the Sommerfeld coefficient shows that when magnetic field exceeds 4T, the system is in gapless superconducting state with only

one non-zero order parameter component.

II. EXPERIMENTAL DETAILS

Single crystals of $Ba_{0.05}K_{0.95}Fe_2As_2$ with typical dimensions $1.3 \times 0.4 \times 0.2$ mm^3 were grown using the K-As flux method[33]. The doping level of the crystals used in this study was determined based on previously reported $T_c - x$ phase diagram[34–36]. The specific heat C and electrical resistivity ρ were measured as a function of temperature T and magnetic field H with $H||c$ and $H||a$ crystallographic axes. $C(T,H)$ was measured using a relaxation technique in a field cooled manner by decreasing the temperature down to 0.5 K for $H||a$ axis and to 2 K for $H||c$ axis. The resistivity measurements were carried out on samples with an *ac* electrical current I_b flowing along the b crystallographic axis and with $H||a$ always perpendicular to I_b. Since these crystals are tetragonal, the a and b directions are in fact equivalent.

III. RESULTS AND DISCUSSION

A. Temperature dependence of the specific heat

Measurements of the specific heat provide an effective way to reveal the structure and the symmetry of the SC gap. Importantly, the magnetic-field dependence of the zero-temperature electronic specific heat coefficient (γ) measured in the mixed state with $H||c$ captures the details of nodal character of the gap symmetry. e.g., Volovik's theory predicts a $\sqrt{H}$ dependence of γ in the case of a d-wave order parameter[37]. However, the presence of $\sqrt{H}$ does not guarantee the nodal character of the gap and can arise due to other reasons. For example, a recent theoretical study of the $s^{\pm}$-wave state in iron-based superconductors shows that a change in the sign of the SC order parameter across different Fermi pockets also leads to the $\sqrt{H}$ dependence of γ[38].

On Figure 1 we show the C/T data vs T for $Ba_{0.05}K_{0.95}Fe_2As_2$ measured in zero field. The superconducting transition region has a width of about 1 K, which is typical for the overdoped samples of this family[36,39–41]. For the unambiguous determination of the thermodynamic superconducting transition temperature T_c we use the *isoentropic* construction (dotted blue line in the main panel), i.e., we choose T_c such as the entropy around the transition is conserved.

Notice that the data of Fig. 1 show a clear shoulder at low temperatures ($T < 2$ K). A similar feature has been observed in other multiband superconductors and it is indicative of the presence of additional SC gap(s) appearing at low temperatures (see e.g.,[42]). In fact, previous publications on KFe_2As_2 have shown that there are at least three gaps present in this system[12,43].

Also notice that there is no low temperature upturn (Schottky nuclear contribution) in any of the specific heat

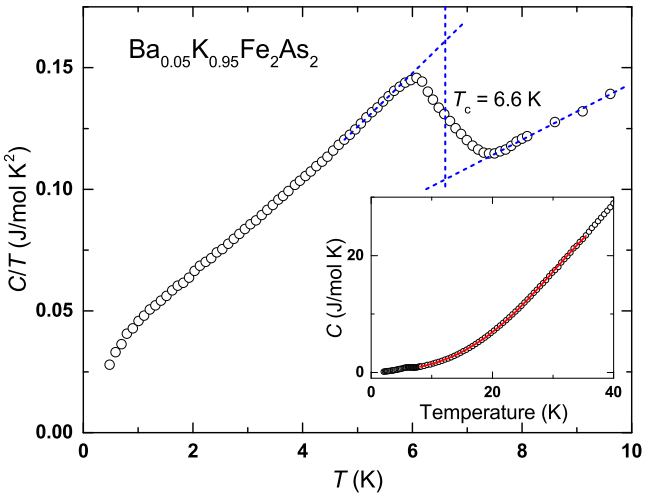

FIG. 1. (Color online) Temperature dependence of C/T for $Ba_{0.05}K_{0.95}Fe_2As_2$ measured in the temperature range 0.5 K$\leq T \leq$ 10 K. The dotted line represents the isoentropic construction used to determine T_c. The inset shows a fit of normal state specific heat C data using an expression $C = \gamma_n T + \beta T^3$ (8 K$\leq T \leq$ 35 K), which is performed to determine the phonon contribution to the measured specific heat.

data measured to temperatures as low as 0.5 K and fields $H||a$ axis up to 14 T. Thus, the measured specific heat can be expressed in terms of electronic and lattice contributions as $C \equiv C_e + C_{ph}$. A fit of the normal state (8 K$\leq T \leq$ 35 K) specific heat data with $C = \gamma_n T + \beta T^3$ gives $\gamma_n = 80$ mJ/mol·K^2 and $\beta = 0.79$ mJ/mol·K^4. The inset to Fig. 1 shows the quality of this fit. The obtained γ_n value is comparable to the values of 69-103 mJ/mol K^2 for KFe_2As_2[27,36,39,44,45] and it is slightly higher than the range 50-60 mJ/mol K^2 of the optimally doped ($x = 0.4$) samples[46,47]. Based on the β value, we obtained a Debye temperature $\theta_D = 230$ K. To determine the electronic contribution to the specific heat, we subtracted the lattice contribution βT^3 from the measured specific heat.

To extract the values of the superconducting gaps from the specific heat data of $Ba_{0.05}K_{0.95}Fe_2As_2$, we plot the electronic specific heat normalized to its normal-state value vs T/T_c (Fig. 2). This plot shows that the specific heat decreases linearly with decreasing temperature over the range $0.2\ T_c \leq T \leq 0.85\ T_c$ followed by a sharp drop around $T = 0.15\ T_c$. This overall T dependence is very similar to that of KFe_2As_2[27,39,45]. The solid green line on the figure is a fit of these data using the BCS model generalized to three bands[48,49] thus, for the time being, assuming that the superconducting order parameter is isotropic on all three Fermi pockets, which ignores both the fact that the intermediate gap may be nodal[12] and the effect of disorder that might induce in-gap states). The details of the procedure used to determine the three gaps by fitting these data with Eq. (2) are discussed in the next paragraph. Notice the excellent fit of the data with this expression. The gap values are $\Delta_{0i} = 1.93$,

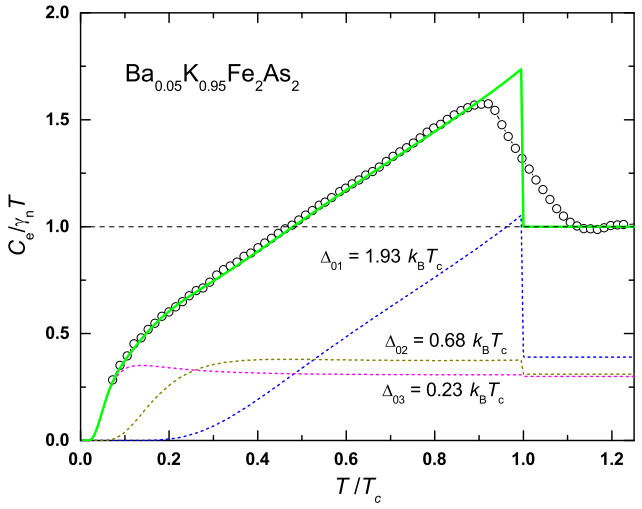

FIG. 2. (Color online) Plot of the electronic specific heat normalized to its normal state value $C_e/\gamma_n T$ vs normalized temperature T/T_c (open circle). The solid green line is a fit of the data using the BCS model generalized to three bands (see text). The three dashed lines show the contribution of the three individual superconducting gaps.

0.68, and 0.23 $k_{\rm B}T_c$. The other fitting parameters are $r_1 = 0.39$, $r_2 = 0.31$, and $r_3 = 0.30$. Separate plots of the contribution of each gap (dashed lines on the figure) show that the smallest gap dominates at low T, while the largest gap gives the linear T dependence. For this reason, our analysis of $C_e(T)$ using the *isotropic* BCS model gives the correct values of these gaps even though the intermediate gap is nodal.

We remind the reader that within the BCS theory of superconductivity, for the case of an isotropic superconductor, the temperature dependence of the order parameter is determined self-consistently from the following results in the two limiting cases: $\Delta(T) \propto \sqrt{(T_c - T)/T_c}$ at $T \sim T_c$ and $\Delta(T) \approx \Delta_0[1 - \sqrt{2\pi T/\Delta_0}\exp(-\Delta_0/k_B T)]$ for $T \ll T_c$. Consequently, the temperature dependence of the entropy S is given by[50]:

$$S = -\frac{6\gamma_n}{\pi^2 k_B}\int_0^\infty [f_\epsilon \ln f_\epsilon + (1-f_\epsilon)\ln(1-f_\epsilon)]d\epsilon, \quad (1)$$

where integration is over single particle energies ϵ, and $f_\epsilon = [\exp(\sqrt{\epsilon^2 + \Delta^2(T)}/k_B T) + 1]^{-1}$ is the Fermi-Dirac distribution function. The electronic specific heat is calculated using the standard thermodynamic expression $C_e = T(\partial S/\partial T)_V$. Based on this, we used a superposition of three different SC gaps Δ_{0i} (i = 1, 2, 3), hence three different C_e with different relative contribution weights r_i:

$$C_e(T) = \sum_{i=1}^{3} r_i C_e(\Delta_{0i}, T). \quad (2)$$

Next, we compare the gap values obtained from our analysis with the previously reported values for KFe_2As_2[12,43]. Specifically, Table 1 lists the gap values from ARPES [12], $C(T)$ of present study, and small angle neutron scattering (SANS)[43]. Notice that in all three cases there is a leading gap that is significantly larger than the other two gaps. Furthermore, our analysis and the SANS study give almost the same values for the three gaps, while the ratios of consecutive gap values (e.g., Δ_{01}/Δ_{02} and Δ_{02}/Δ_{03}) are around 2.8 for both ARPES and our $C(T)$ study. We also note that the ARPES results have shown that the three components of the superconducting order parameter correspond to the three hole pockets near the Γ point, with a nodal intermediate gap and a nodeless leading gap that is significantly larger than the other two. On the other hand, the superconducting gaps detected in dHvA measurements on $Ba_{0.07}K_{0.93}Fe_2As_2$ are all around Γ point[51]. A comparison of all these findings implies that the superconducting order parameter of $Ba_{0.05}K_{0.95}Fe_2As_2$ has three different components, centered around the Γ point with the values given above and with the middle gap nodal, but, as we will show later, most likely they are not protected by symmetry.

TABLE I. The superconducting gap values of $Ba_{1-x}K_xFe_2As_2$ obtained in this study for the $x = 0.95$ sample are compared with those reported in ARPES and SANS for the $x = 1$ sample. The gaps are given in units of $k_{\rm B}T_c$.

ARPES		C(T)	SANS
$x = 1$ Ref. [12]		$x = 0.95$	$x = 1$ Ref. [43]
3.8	inner	1.93	1.77
1.4	middle	0.68	0.72
0.5	outer	0.23	0.21

B. Magnetic field dependence of the specific heat

Next, we show the results of the magnetic field dependence of the specific heat for $H||a$ axis. Figure 3 shows the temperature dependence of C/T for different H values for the $Ba_{0.05}K_{0.95}Fe_2As_2$ sample. The low temperature data (see inset to Fig. 3) clearly show that the behavior of C/T vs T is very different at low and high magnetic fields: a shoulder in C/T is observed at low fields, while it varies quadratically in T at high fields. As discussed before, the shoulder in C/T is typical of multiband superconductors, with additional gap(s) being present at low T and H. The quadratic temperature dependence at high fields is due to the lattice contribution to the specific heat and, as such, it is of no great interest here.

The field dependence of the zero-temperature Sommerfeld coefficient γ for $H||a$ axis, in principle, allows us to probe the relative sign between two components of the superconducting order parameter, assuming that the third

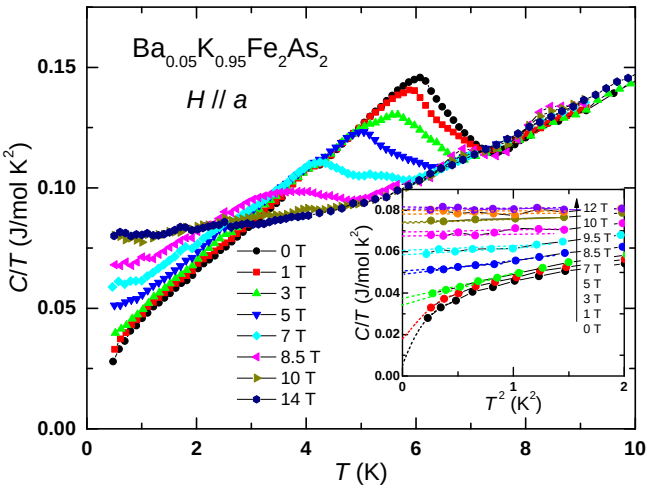

FIG. 3. (Color online) Temperature T dependence of the specific heat C/T of $Ba_{0.05}K_{0.95}Fe_2As_2$ measured for 0.5 K $\leqslant$ T $\leqslant$ 10 K and magnetic fields $0 \leq H \leq 14$ T with $H||a$ axis. Inset: C/T as a function of T^2 measured at low temperatures. An extrapolation (dashed lines) of these data at $T = 0$ gives the zero-temperature Sommerfeld coefficient γ. Only selected fields are shown on both figures.

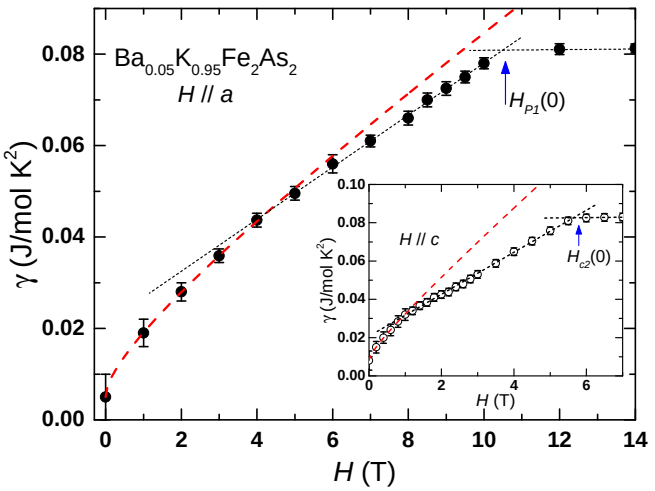

FIG. 4. (Color online) Magnetic field H dependence of the zero-temperature Sommerfeld coefficient γ of $Ba_{0.05}K_{0.95}Fe_2As_2$ for $H||a$ axis and $H||c$ axis (inset). The red dashed line is a fit of the low H data with Eq. (3), while the black dotted line is a linear fit of the high H data. The $H_{P1}(0)$ and $H_{c2}(0)$ represent the upper critical field with field applied parallel to a and c axis, respectively.

component has been fully suppressed by the magnetic field. We obtained the magnetic-field dependence of γ (Fig. 4) by extrapolating the data shown in the inset to Fig. 3 to zero temperature. Notice the excellent fit of the data for $H \leq 4$ T (red dashed line) with

$$\gamma = a \cdot \sqrt{H} + b \cdot H + c, \qquad (3)$$

where $a = 0.009$ J/(mol K^{2}T$^{1/2}$), $b = 0.005$ J/(mol K^2 T) and $c = 0.005$ J/(mol K^2). The non-zero value of c indicates the presence of disorder-induced scattering which involves the values of momenta where the order parameter vanishes. The impurity amount is about 6% since this value of c is only 6% of γ_n. As we discuss in detail in the next paragraph, the $\sqrt{H}$ dependence at low fields is the result of the change in the sign of the SC order parameter across different Fermi pockets[38] and also emphasizes the role of disorder-induced scattering.

Physically, the $\sqrt{H}$ dependence of γ for $H < 4$ T can be interpreted as follows. Let us formally consider the superconducting order parameter $\Delta(\mathbf{k})$ which is defined everywhere in the Brillouin zone. Then, consider two Fermi sheets FS_1 and FS_2 on which the order parameter has opposite sign: $\Delta(\mathbf{k}_{FS_1}) = |\Delta_{01}|$ and $\Delta(\mathbf{k}_{FS_2}) = -|\Delta_{02}|$. Clearly, on an arbitrary line connecting the two Fermi sheets in momentum space there is a point $\mathbf{k}_0$ where the order parameter vanishes, $\Delta(\mathbf{k}_0) = 0$. In the presence of disorder, single particle scattering can involve states with momentum transfers that involve parts of the Brillouin zone between the different Fermi sheets where the order parameter vanishes. These scattering processes effectively mimic the presence of nodes in the superconducting order parameter, resulting in the $\sqrt{H}$ dependence of γ at lower fields, instead of the expected linear-in-H behavior[38]. Also, note that, when the Fermi sheets are sufficiently close to each other, as is the case in $Ba_{0.05}K_{0.95}Fe_2As_2$, the disorder does not necessarily have to be strong, unlike in the case when the relevant Fermi sheets are significantly separated in the BZ, say, one is around Γ point, while another one is around M point. Therefore, a 6% disorder, as observed for this doping, seems to be sufficient to give the $\sqrt{H}$ dependence in $\gamma(H)$, i.e., to mimic the presence of nodes. We also note that, although in general, for a fixed magnetic field parallel to the FeAs planes, specific heat experiment cannot directly probe the nodal structure for each component of the order parameter, it can still probe whether the current lines pass through parts of the Fermi sheets with different or same sign of the corresponding pairing component and measure the relative sign of the order parameter components, provided the disorder-induced scattering is present in the system. Moreover, the above theoretical approach based on the Volovik's effect implies that the orbital effect is the dominant pair-braking mechanism. As we will show later (Fig. 6), in $Ba_{0.05}K_{0.95}Fe_2As_2$ with $H||a$ axis, the orbital effect dominates at low fields, while Zeeman effect is the dominant pair breaker at high fields.

This result when compared with the other studies, including the most recent one by Kim et al.[28], can in principle be interpreted as evidence that the nodal structure of the intermediate component of the order parameter is most likely not symmetry protected, i.e., the nodes are accidental. In fact, recent theoretical studies[5], specifically addressing the structure of the superconducting gap in KFe_2As_2, show that the states with and without acci-

dental nodes are very close to degeneracy.

We determine the Pauli limiting field $H_{P2}(0)$ for the $\Delta_{02} = 0.68\ k_BT_c$ gap as follows. It is well known that there is a linear correlation between $H_{c2}(0)$ and the superconducting gap Δ_0 if the Pauli paramagnetic limit is the dominant pair-breaking mechanism, which is the case when $H||a$ axis. Thus, we get $H_{P2}(0) = 3.7$ T for the gap $\Delta_{02} = 0.68\ k_BT_c$ if we take $H_{P1}(0) = 10.5$ T (see Fig. 4) for the largest gap $\Delta_{01} = 1.93\ k_BT_c$. The fact that this value is very close to 4 T, where there is the crossover between the sublinear and the linear in H dependence of γ (see Fig. 4), further shows that the order parameter has only one non-zero component for $H > H_{P2}$, so that the system is in a gapless superconducting state[52]. A detailed study of this state will be the focus of future work.

We also determined the field dependence of the zero-temperature γ with $H||c$ axis (see inset to Fig. 4) using the same method as used for $H||a$ axis. This inset shows an apparent change of γ around 1 T. Thus, the fit using Eq. (3) for $H \leq 1$ T gives $a = 0.009$ J/(mol K^{2}T$^{1/2}$), $b = 0.016$ J/(mol K^{2}T), and $c = 0.008$ J/(mol K^2). The values of these fitting parameters are comparable with those obtained for $H||a$ axis. Such a $\sqrt{H}$ dependence of γ for $H||c$ was also observed in other high-doping crystals and is well explained using Volovik's theory[37]. In this configuration, the orbital effect is dominant in the pair-breaking mechanism, hence, there is a quadratic correlation between $H_{c2}(0)$ and Δ, i.e., $H_{c2}(0) \propto \Delta^2$. Thus, we calculated $H_{c2}(0) = 0.75$ T for the gap $\Delta_{02} = 0.68k_BT_c$ if we take $H_{c2}(0) = 6$ T (see the inset to Fig. 4) for the largest gap $\Delta_{01} = 1.93k_BT_c$. This estimated $H_{c2}(0)$ value is very close to the change of γ around 1 T, indicating that this change is caused by the close of the 0.68 k_BT_c superconducting gap. Above ~1 T, a linear-like field dependence is observed after the system is in a gapless superconducting state. All these results show the excellent agreement between the results with $H||a$ and $H||c$ axes and also show the consistency of the analysis used.

In general, the field dependence of γ is different for $H||a$ and $H||c$ axes since in the former (latter) case the Zeeman (orbital) effect dominates the pair-braking mechanism. Hence, the fact that $\gamma(H)$ is similar for $H||a$ and $H||c$ axes furthermore indicates that the orbital effect, manifested through the $\sqrt{H}$ behavior, plays an important role in the low-H regime when $H||a$ axis, in agreement with the recent experimental finding of Josephson vortices in iron-based superconductors[53].

C. H-T phase diagram

For magnetic fields $H||a$ axis, one generally expects a competition between the pair breaking processes due to Zeeman and orbital effects. However, as we discussed above, our data for $\gamma(H)$ (Fig. 4) clearly shows a crossover behavior from orbital dominated regime at low fields ($H < 4$ T) to Zeeman effect dominated regime at high fields, suggesting an interplay between the momentum and spin degrees of freedom. In iron-pnictide superconductors this problem is well defined thanks to the negligibly small magnitude of the spin-orbit coupling. The presence of such an interplay is somewhat surprising given that the field configuration $H||a$ axis should lead to the much more dominant role of the Pauli limiting effects down to small magnetic fields just as it happens in the '115' heavy-fermion superconductors such as $CeCoIn_5$. In order to quantify the contributions the orbital and Pauli limiting effects, we study the temperature dependence of the upper critical field $H_{c2}^{||}(T)$ for $H||a$ axis.

The superconducting critical temperatures under different fields with $H||a$ and $H||c$ axes were determined using the isoentropic method discuss earlier and shown in

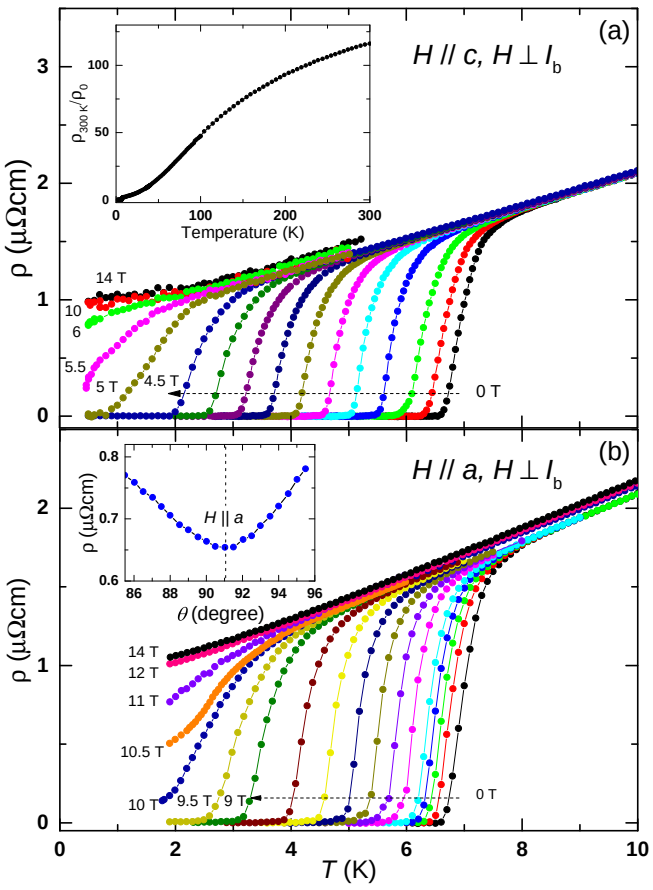

FIG. 5. (Color online) Temperature dependence of electrical resistivity $\rho(T)$ of $Ba_{0.05}K_{0.95}Fe_2As_2$ in magnetic field up to 14 T with (a) $H||c$ and (b) $H||a$. The direction of magnetic field H is always perpendicular to the electrical current I_b. For $H||c$, H is 0, 0.2, 0.5 T and increases from 0.5 to 6 T in steps of 0.5 T. For $H||a$, H increases in steps of 0.5 T between 0 and 2, and 1 T between 2 to 9 T. Insets of (a) and (b): T dependence of resistivity at high temperature showing an $RRR > 100$ and angular dependence of ρ around $H||a$ that is used to estimate the misalignment, respectively.

Fig. 1. Since the SC transition region in $C(T,H)$ broadens with increasing H (see Fig. 3), it becomes considerably difficult to determine the thermodynamic $T_c(H)$ at high H values from $C(T,H)$. Thus, we determined $T_c(H)$ from the resistivity $\rho(T,H)$ data, as discussed in a following paragraph. Plots of $\rho(T,H)$ with $H||c$ and $H||a$ axes are shown in Figs. 5(a) and 5(b), respectively. In both configurations, the magnetic field was always applied perpendicular to the current I_b. The angular θ dependence of ρ at constant H and T [inset to Fig. 5(b)] shows that the misalignment between H and the a axis of the single crystal in our experiments is less than 2°. Nevertheless, we carried out the measurements of $\rho(T)$ with $H||c$ and $H||a$ after correcting for this misalignment. The $\rho(T,H)$ curves shift to lower T with increasing H. The substantial broadening of the transition for $H \geq 4$ T for $H||c$ axis and $H \geq 8$ T for $H||a$ axis is a result of the dissipation of Abrikosov and Josephson vortices, respectively.

As shown in the inset to Fig. 5(a), the residual resistivity ratio $RRR = \rho_{300\mathrm{K}}/\rho_0$ is as large as 120, where $\rho_0 \sim 1\mu\Omega$cm. The RRR value is comparable with the values obtained in other reported high quality single crystals with doping level $x < 1$, but much smaller than the extremely high value found in KFe_2As_2 (more than 2000)[54]. The RRR value of our crystal shows that it is weakly disordered compared with the KFe_2As_2. The 10-90% width of the transition in $\rho(T)$ for $H = 0$ is within 0.5 K, implying the sharpness of the superconducting transition and it further confirms the high quality of the sample.

We determined $T_c(H)$ from the resistivity $\rho(T,H)$ data as the temperature of zero resistivity (data not shown) since we noticed that the zero-field T_c determined from heat capacity corresponds to to the zero-value resistivity. This result is reasonable because the width of the transition in *zero applied magnetic field* (~ 0.5 K) is most likely a result of sample inhomogeneity. The difference between $T_c(H)$ determined from resistivity and specific heat increases linearly with increasing field. This behavior is a result of the increase of the number of vortices, hence, of the vortex contribution to dissipation, with increasing H. Thus, the zero-resistivity $T_c(H)$ at higher field values is underestimating the thermodynamic $T_c(H)$. Nevertheless, the observed linear correlation allows us to correct for the underestimated $T_c(H)$ extracted from $\rho(H,T)$. The resulting H-T phase diagram obtained from $C(T,H)$ and $\rho(T,H)$ with both $H||c$ and $H||a$ axes is shown in Fig. 5 after correcting for the underestimation of the $T_c(H)$ determined from $\rho(T,H)$.

The Werthamer-Helfand-Hohenberg-Maki (WHHM) model[55,56] has been known as a useful theoretical prescription to evaluate $H_{c2}(T)$. Importantly, the model includes the effects of Pauli spin paramagnetism, spin-orbit scattering, and orbital diamagnetic effects. We fit out data with a single-band WHHM model using the following expression:

$$\ln\frac{T_c}{T} = \mathrm{Re}\left\{\psi\left[\frac{1}{2}+(1+i\alpha)\frac{hT}{2T_c}\right]\right\} - \psi\left(\frac{1}{2}\right), \qquad (4)$$

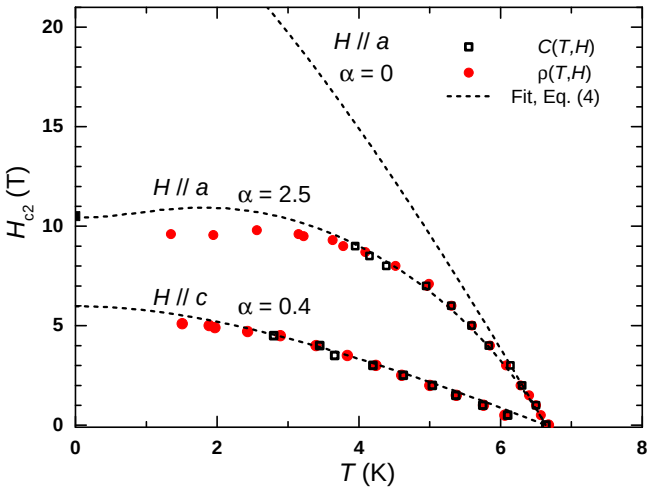

FIG. 6. (Color online) Upper critical field H_{c2} vs T phase diagram of $Ba_{0.05}K_{0.95}Fe_2As_2$. The dashed lines are fits of the data with the WHHM model ignoring the spin-orbit coupling contribution, i.e., $\lambda = 0$ [see discussion for Eq. (4) for details].

where $h = 4H_{c2}/[-\pi^2 T_c(\mathrm{d}H_{c2}/\mathrm{d}T)_{T=T_c}]$, $\psi(z)$ is digamma function, and α [$= \sqrt{2}H_{c2}^{\mathrm{orb}}(0)/H_{c2}^{\mathrm{pm}}(0)$] is Maki parameter that accounts for the relative contribution of orbital effect and Pauli spin paramagnetism[57,58]. In Eq. (4) we ignore the effect of spin-orbit coupling. Fits of the data with Eq. (4) (dotted lines) give $\alpha = 2.5$ for $H||a$ axis and $\alpha = 0.4$ for $H||c$ axis. These values for the Maki parameter are comparable to those obtained for the stoichiometric KFe_2As_2[59–61]. Notice the excellent agreement between the $H_{c2}(T)$ data and these fits. They yield $H_{c2}^{||}(0) \approx 10.5$ and $H_{c2}^{\perp} \approx 6.0$ T for $H||a$ and $H||c$ axis, respectively. We note that the value $H_{c2}^{||}(0) \approx 10.5$ T obtained from Eq. (4) is in very good agreement with $H_{P1}(0) = 10.5$ T obtained from $\gamma(H)$ shown on Fig. 4.

The orbital limit at zero temperature and in the dirty limit is $H_{c2}^{\mathrm{orb}}(0) = -0.69T_c(\mathrm{d}H/\mathrm{d}T)_{T=T_c} = 27.5$ T ($T_c = 6.6$ K) for $H||a$ axis, much larger that $H_{c2}^{||}(0) \approx 10.5$, and $H_{c2}^{\mathrm{orb}}(0) = 6.4$ T for $H||c$, comparable with $H_{c2}^{\perp} \approx 6.0$ T. We also calculated the orbital effect with $H||a$ axis using Eq. (4) with $\alpha = 0$, also shown in Fig. 4 as a dotted line. Notice that this latter result only reproduces the $H_{c2}(T)$ data at low fields ($H < 3.5$ T). In summary, all these results clearly show that, for $H||a$ axis, the orbital effects dominate at low fields ($H < 3.5$ T) and the Pauli paramagnetic limit dominates at high fields, while for $H||c$ the orbital limit is dominant over the whole field range.

One can also calculate the value of α in the dirty limit using the expression[55]

$$\alpha = 3e^2\hbar\gamma_n\rho_n/2m\pi k_{\mathrm{B}}^2, \qquad (5)$$

where γ_n and ρ_n are the specific heat coefficient and resistivity in the normal state (at T_c), respectively. With the previously determined values of $\gamma_n \approx 80$ mJ/mol K^2 and $\rho_n = 1.8$ $\mu\Omega$cm for $H||a$ axis, Eq. (5) gives $\alpha =$

2.4±0.1. This value is in excellent agreement with the one obtained by fitting the data of Fig. 6 for $H||a$ with Eq. (4).

Another interesting feature of the data of Fig. 6 for $H||a$ is the re-entrance region at small temperatures. Usually, this type of behavior is a signature for an instability which ultimately results in a first order transition manifested in discontinuous changes in thermodynamic quantities such as magnetization or thermal expansion coefficient. Interestingly, such a transition has, indeed, been observed in KFe_2As_2[59]. This suggests again that the physics of the heavily hole-doped compound $Ba_{0.05}K_{0.95}Fe_2As_2$ is very similar to the physics of KFe_2As_2. However, the detailed investigation of a first order transition in magnetic field goes beyond the scope of this paper.

IV. SUMMARY

In summary, we have studied the bulk properties of $Ba_{0.05}K_{0.95}Fe_2As_2$, which is between the Lifshitz transition (around ∼0.9) and the stoichiometric KFe_2As_2. We show that the specific heat $C(T)$ can be fitted using the BCS theory generalized to the presence of three bands and extract the three gap values as $\Delta_{0i} = 1.93$, 0.68, and 0.23 k_BT_c. We also discussed the magnetic field dependence of the zero-temperature Sommerfeld coefficient $\gamma(H)$ with $H||a$ and show that at least two of the three order parameter components have opposite signs. Our analysis of $\gamma(H)$ reveals a gapless superconducting state at a magnetic field higher than the $H_{c2} \approx 4$ T, while the nodes previously reported in the intermediate component of the order parameter are most likely accidental. The $H_{c2} - T$ phase diagram is obtained from the resistivity and specific heat data and is analyzed using the WHHM theory. We found that the orbital effects provide the dominant pair-breaking mechanism at the low-H regime with $H||a$. We observed remarkable similarities between the thermodynamic and magnetic properties of $Ba_{0.05}K_{0.95}Fe_2As_2$ and stoichiometric compound KFe_2As_2.

ACKNOWLEDGMENTS

This work has been supported by the National Science Foundation NSF DMR-1505826 at Kent State University. M.D. acknowledges financial support from KSU and MPI-PKS.

[1] D. F. Agterberg, V. Barzykin, and L. P. Gor'kov, Phys. Rev. B **60**, 14868 (1999).
[2] M. Rotter, M. Tegel, and D. Johrendt, Phys. Rev. Lett. **101**, 107006 (2008).
[3] W.-C. Lee, S.-C. Zhang, and C. Wu, Phys. Rev. Lett. **102**, 217002 (2009).
[4] M. A. Tanatar, J.-P. Reid, H. Shakeripour, X. G. Luo, N. Doiron-Leyraud, N. Ni, S. L. Bud'ko, P. C. Canfield, R. Prozorov, and L. Taillefer, Phys. Rev. Lett. **104**, 067002 (2010).
[5] S. Maiti, M. M. Korshunov, and A. V. Chubukov, Phys. Rev. B **85**, 014511 (2012).
[6] S. Maiti and A. V. Chubukov, Phys. Rev. B **87**, 144511 (2013).
[7] J. Garaud and E. Babaev, Phys. Rev. Lett. **112**, 017003 (2014).
[8] J. Kang, A. F. Kemper, and R. M. Fernandes, Phys. Rev. Lett. **113**, 217001 (2014).
[9] H. Ding, P. Richard, K. Nakayama, K. Sugawara, T. Arakane, Y. Sekiba, A. Takayama, S. Souma, T. Sato, T. Takahashi, Z. Wang, X. Dai, Z. Fang, G. F. Chen, J. L. Luo, and N. L. Wang, EPL (Europhysics Letters) **83**, 47001 (2008).
[10] T. Shimojima, F. Sakaguchi, K. Ishizaka, Y. Ishida, T. Kiss, M. Okawa, T. Togashi, C.-T. Chen, S. Watanabe, M. Arita, K. Shimada, H. Namatame, M. Taniguchi, K. Ohgushi, S. Kasahara, T. Terashima, T. Shibauchi, Y. Matsuda, A. Chainani, and S. Shin, Science **332**, 564 (2011).
[11] K. Hashimoto, A. Serafin, S. Tonegawa, R. Katsumata, R. Okazaki, T. Saito, H. Fukazawa, Y. Kohori, K. Kihou, C. H. Lee, A. Iyo, H. Eisaki, H. Ikeda, Y. Matsuda, A. Carrington, and T. Shibauchi, Phys. Rev. B **82**, 014526 (2010).
[12] K. Okazaki, Y. Ota, Y. Kotani, W. Malaeb, Y. Ishida, T. Shimojima, T. Kiss, S. Watanabe, C.-T. Chen, K. Kihou, C. H. Lee, A. Iyo, H. Eisaki, T. Saito, H. Fukazawa, Y. Kohori, K. Hashimoto, T. Shibauchi, Y. Matsuda, H. Ikeda, H. Miyahara, R. Arita, A. Chainani, and S. Shin, Science **337**, 1314 (2012).
[13] F. F. Tafti, A. Juneau-Fecteau, M.-E. Delage, S. Rene de Cotret, J.-P. Reid, A. F. Wang, X.-G. Luo, X. H. Chen, N. Doiron-Leyraud, and L. Taillefer, Nat Phys **9**, 349 (2013).
[14] D. Watanabe, T. Yamashita, Y. Kawamoto, S. Kurata, Y. Mizukami, T. Ohta, S. Kasahara, M. Yamashita, T. Saito, H. Fukazawa, Y. Kohori, S. Ishida, K. Kihou, C. H. Lee, A. Iyo, H. Eisaki, A. B. Vorontsov, T. Shibauchi, and Y. Matsuda, Phys. Rev. B **89**, 115112 (2014).
[15] T. Sato, K. Nakayama, Y. Sekiba, P. Richard, Y.-M. Xu, S. Souma, T. Takahashi, G. F. Chen, J. L. Luo, N. L. Wang, and H. Ding, Phys. Rev. Lett. **103**, 047002 (2009).
[16] I. I. Mazin, Nature **464**, 183 (2010).
[17] Z. P. Yin, K. Haule, and G. Kotliar, Nature Materials **10**, 932 (2011).
[18] W.-C. Lee, S.-C. Zhang, and C. Wu, Phys. Rev. Lett. **102**, 217002 (2009).
[19] S. Graser, A. F. Kemper, T. A. Maier, H.-P. Cheng, P. J. Hirschfeld, and D. J. Scalapino, Phys. Rev. B **81**, 214503 (2010).
[20] R. Thomale, C. Platt, W. Hanke, J. Hu, and B. A. Bernevig, Phys. Rev. Lett. **107**, 117001 (2011).
[21] R. M. Fernandes and A. J. Millis, Phys. Rev. Lett. **110**, 117004 (2013).

[22] S. N. Khan and D. D. Johnson, Phys. Rev. Lett. **112**, 156401 (2014).
[23] H. Hodovanets, Y. Liu, A. Jesche, S. Ran, E. D. Mun, T. A. Lograsso, S. L. Bud'ko, and P. C. Canfield, Phys. Rev. B **89**, 224517 (2014).
[24] N. Xu, P. Richard, X. Shi, A. van Roekeghem, T. Qian, E. Razzoli, E. Rienks, G.-F. Chen, E. Ieki, K. Nakayama, T. Sato, T. Takahashi, M. Shi, and H. Ding, Phys. Rev. B **88**, 220508 (2013).
[25] Y. Ota, K. Okazaki, Y. Kotani, T. Shimojima, W. Malaeb, S. Watanabe, C.-T. Chen, K. Kihou, C. H. Lee, A. Iyo, H. Eisaki, T. Saito, H. Fukazawa, Y. Kohori, and S. Shin, Phys. Rev. B **89**, 081103 (2014).
[26] F. Hardy, R. Eder, M. Jackson, D. Aoki, C. Paulsen, T. Wolf, P. Burger, A. Bhmer, P. Schweiss, P. Adelmann, R. A. Fisher, and C. Meingast, J. Phys. Soc. Jpn. **83**, 014711 (2014).
[27] F. Hardy, A. E. Böhmer, D. Aoki, P. Burger, T. Wolf, P. Schweiss, R. Heid, P. Adelmann, Y. X. Yao, G. Kotliar, J. Schmalian, and C. Meingast, Phys. Rev. Lett. **111**, 027002 (2013).
[28] J. S. Kim, G. R. Stewart, Y. Liu, and T. A. Lograsso, Phys. Rev. B **91**, 214506 (2015).
[29] J.-P. Reid, M. A. Tanatar, A. Juneau-Fecteau, R. T. Gordon, S. R. de Cotret, N. Doiron-Leyraud, T. Saito, H. Fukazawa, Y. Kohori, K. Kihou, C. H. Lee, A. Iyo, H. Eisaki, R. Prozorov, and L. Taillefer, Phys. Rev. Lett. **109**, 087001 (2012).
[30] J.-P. Reid, A. Juneau-Fecteau, R. T. Gordon, S. R. de Cotret, N. Doiron-Leyraud, X. G. Luo, H. Shakeripour, J. Chang, M. A. Tanatar, H. Kim, R. Prozorov, T. Saito, H. Fukazawa, Y. Kohori, K. Kihou, C. H. Lee, A. Iyo, H. Eisaki, B. Shen, H.-H. Wen, and L. Taillefer, Supercond. Sci. Technol. **25**, 084013 (2012).
[31] H. Kim, M. A. Tanatar, Y. Liu, Z. C. Sims, C. Zhang, P. Dai, T. A. Lograsso, and R. Prozorov, Phys. Rev. B **89**, 174519 (2014).
[32] V. Grinenko, D. V. Efremov, S.-L. Drechsler, S. Aswartham, D. Gruner, M. Roslova, I. Morozov, K. Nenkov, S. Wurmehl, A. U. B. Wolter, B. Holzapfel, and B. Büchner, Phys. Rev. B **89**, 060504 (2014).
[33] K. Kihou, T. Saito, S. Ishida, M. Nakajima, Y. Tomioka, H. Fukazawa, Y. Kohori, T. Ito, S.-i. Uchida, A. Iyo, C.-H. Lee, and H. Eisaki, J. Phys. Soc. Jpn. **79**, 124713 (2010).
[34] M. Rotter, M. Pangerl, M. Tegel, and D. Johrendt, Angew. Chem. Int. Ed. **47**, 7949 (2008).
[35] S. Avci, O. Chmaissem, D. Y. Chung, S. Rosenkranz, E. A. Goremychkin, J. P. Castellan, I. S. Todorov, J. A. Schlueter, H. Claus, A. Daoud-Aladine, D. D. Khalyavin, M. G. Kanatzidis, and R. Osborn, Phys. Rev. B **85**, 184507 (2012).
[36] J. G. Storey, J. W. Loram, J. R. Cooper, Z. Bukowski, and J. Karpinski, Phys. Rev. B **88**, 144502 (2013).
[37] V. G. E., JETP Lett. **58**, 496 (1993).
[38] Y. Bang, Phys. Rev. Lett. **104**, 217001 (2010).
[39] M. Abdel-Hafiez, S. Aswartham, S. Wurmehl, V. Grinenko, C. Hess, S.-L. Drechsler, S. Johnston, A. U. B. Wolter, B. Büchner, H. Rosner, and L. Boeri, Phys. Rev. B **85**, 134533 (2012).
[40] S. L. Bud'ko, Y. Liu, T. A. Lograsso, and P. C. Canfield, Phys. Rev. B **86**, 224514 (2012).
[41] S. L. Bud'ko, M. Sturza, D. Y. Chung, M. G. Kanatzidis, and P. C. Canfield, Phys. Rev. B **87**, 100509 (2013).
[42] F. Bouquet, R. A. Fisher, N. E. Phillips, D. G. Hinks, and J. D. Jorgensen, Phys. Rev. Lett. **87**, 047001 (2001).
[43] H. Kawano-Furukawa, C. J. Bowell, J. S. White, R. W. Heslop, A. S. Cameron, E. M. Forgan, K. Kihou, C. H. Lee, A. Iyo, H. Eisaki, T. Saito, H. Fukazawa, Y. Kohori, R. Cubitt, C. D. Dewhurst, J. L. Gavilano, and M. Zolliker, Phys. Rev. B **84**, 024507 (2011).
[44] H. Fukazawa, Y. Yamada, K. Kondo, T. Saito, Y. Kohori, K. Kuga, Y. Matsumoto, S. Nakatsuji, H. Kito, P. M. Shirage, K. Kihou, N. Takeshita, C.-H. Lee, A. Iyo, and H. Eisaki, J. Phys. Soc. Jpn. **78**, 083712 (2009).
[45] F. Hardy, R. Eder, M. Jackson, D. Aoki, C. Paulsen, T. Wolf, P. Burger, A. Böhmer, P. Schweiss, P. Adelmann, R. A. Fisher, and C. Meingast, J. Phys. Soc. Jpn. **83**, 014711 (2014).
[46] C. Kant, J. Deisenhofer, A. Günther, F. Schrettle, A. Loidl, M. Rotter, and D. Johrendt, Phys. Rev. B **81**, 014529 (2010).
[47] P. Popovich, A. V. Boris, O. V. Dolgov, A. A. Golubov, D. L. Sun, C. T. Lin, R. K. Kremer, and B. Keimer, Phys. Rev. Lett. **105**, 027003 (2010).
[48] J. Nagamatsu, N. Nakagawa, T. Muranaka, Y. Zenitani, and J. Akimitsu, Nature **410**, 63 (2001).
[49] F. Bouquet, Y. Wang, R. A. Fisher, D. G. Hinks, J. D. Jorgensen, A. Junod, and N. E. Phillips, Europhys. Lett. **56**, 856 (2001).
[50] B. Mühlschlegel, Z. Physik **155**, 313 (1959).
[51] T. Terashima, N. Kurita, M. Kimata, M. Tomita, S. Tsuchiya, M. Imai, A. Sato, K. Kihou, C.-H. Lee, H. Kito, H. Eisaki, A. Iyo, T. Saito, H. Fukazawa, Y. Kohori, H. Harima, and S. Uji, Phys. Rev. B **87**, 224512 (2013).
[52] V. Barzykin and L. P. Gor'kov, Phys. Rev. Lett. **98**, 087004 (2007).
[53] P. J. W. Moll, L. Balicas, V. Geshkenbein, G. Blatter, J. Karpinski, N. D. Zhigadlo, and B. T. Batlogg, Nature Materials **12**, 134 (2013).
[54] Y. Liu, M. A. Tanatar, V. G. Kogan, H. Kim, T. A. Lograsso, and R. Prozorov, Phys. Rev. B **87**, 134513 (2013).
[55] N. R. Werthamer, E. Helfand, and P. C. Hohenberg, Phys. Rev. **147**, 295 (1966).
[56] E. Helfand and N. R. Werthamer, Phys. Rev. **147**, 288 (1966).
[57] K. Maki, Physics **1**, 127 (1964).
[58] K. Maki, Phys. Rev. **148**, 362 (1966).
[59] D. A. Zocco, K. Grube, F. Eilers, T. Wolf, and H. v. Löhneysen, Phys. Rev. Lett. **111**, 057007 (2013).
[60] P. Burger, F. Hardy, D. Aoki, A. E. Böhmer, R. Eder, R. Heid, T. Wolf, P. Schweiss, R. Fromknecht, M. J. Jackson, C. Paulsen, and C. Meingast, Phys. Rev. B **88**, 014517 (2013).
[61] T. Terashima, K. Kihou, M. Tomita, S. Tsuchiya, N. Kikugawa, S. Ishida, C.-H. Lee, A. Iyo, H. Eisaki, and S. Uji, Phys. Rev. B **87**, 184513 (2013).